

Segment Any 4D Gaussians

Shengxiang Ji^{1*}, Guanjun Wu^{1*}, Jiemin Fang², Jiazhong Cen³,
Taoran Yi⁴, Wenyu Liu⁴, Qi Tian², Xinggang Wang^{4†}

¹School of CS, Huazhong University of Science and Technology ²Huawei Inc.

³MoE Key Lab of Artificial Intelligence, AI Institute, Shanghai Jiao Tong University

⁴School of EIC, Huazhong University of Science and Technology

{jishengxiangzs, jaminfang}@gmail.com

{guajuwu, taoranyi, liuwu, xgwang}@hust.edu.cn

jiazhongcen@sjtu.edu.cn, tian.qi1@huawei.com



Figure 1: Applications of SA4D. Given pre-trained 4D Gaussians (column a), SA4D decomposes the Gaussians into the object level and supports object removal/recoloring (column b), composition (column c), and rendering anything masks (column d).

Abstract

Modeling, understanding, and reconstructing the real world are crucial in XR/VR. Recently, 3D Gaussian Splatting (3D-GS) methods have shown remarkable success in modeling and understanding 3D scenes. Similarly, various 4D representations have demonstrated the ability to capture the dynamics of the 4D world. However, there is a dearth of research focusing on segmentation within 4D representations. In this paper, we propose Segment Any 4D Gaussians (SA4D), one of the first frameworks to segment anything in the 4D digital world based on 4D Gaussians. In SA4D, an efficient temporal identity feature field is introduced to handle Gaussian drifting, with the potential to learn precise identity features from noisy and sparse input. Additionally, a 4D segmentation refinement process is proposed to remove artifacts. Our SA4D achieves precise, high-quality segmentation within seconds in 4D Gaussians and shows the ability to remove, recolor, compose, and render high-quality anything masks. More demos are available at: <https://jsxzs.github.io/sa4d/>.

*Equal contributions.

†Corresponding author.

1 Introduction

Recently, SAM [1] has achieved great success in understanding the 2D image, and [2] extends it to the 3D representations. 3D Gaussian Splatting (3D-GS) [3] has proven to be an efficient approach to modeling 3D scenes, which boosts the booming of 3D understanding [4, 5, 6]. However, our world lives in 4D. Therefore, achieving interactive and high-quality segmentation in 4D scenes remains an important and challenging task. We believe that 4D segmentation should achieve two goals: (a) Fast and interactive segmentation across the entire scene and (b) High-quality segmentation results. Some prior works [7, 8, 9, 10] attempt to use binary segmentation masks to separate objects or train dynamic parts individually. However, they struggle to provide interactive and fast object-level segmentation masks. Meanwhile, directly incorporating segmentation features into 3D Gaussians [11, 12, 13] can only address 6-DoF motion, such as cars, and may fall short in capturing non-rigid dynamics.

The first problem in building a 4D segmentation framework is *how to find an efficient solution to lift SAM to 4D representations?* An intuitive solution to building a segmentation framework is to perform 3D segmentation [4, 14, 5] on the **deformed 3D Gaussians**, and then propagate it to the other timestamps using the deformation field of the 4D Gaussians. However, this approach may suffer from *Gaussian drifting*: the non-rigid motion in which some 3D Gaussians belong to one object before timestamp t_0 but become part of another object afterward, as shown in Fig. 2.

To tackle the aforementioned challenges, we propose SA4D, which extends SAM to 4D representations. For precise 4D segmentation, we choose 4D Gaussian Splatting (4D-GS) [15] as the 4D representation. This method explicitly trains an independent Gaussian deformation field for motion and maintains a global canonical 3D Gaussians, allowing the use of sparse semantic features from any other frames at different timestamps, unlike other representations [11, 16] that focus only on local temporal spaces. Since the 4D world is typically captured by videos, we adopt a video object tracking foundation model [17] to generate per-frame identity masks. To efficiently compose sparse and noisy semantic priors, we propose a temporal identity feature field network, which (a) successfully resolves *Gaussian drifting* by predicting time-dependent Gaussian semantic features, and (b) enables learning precise object identity information from noisy inputs of the video object tracking foundation model. After training, we introduce a Gaussian identity table to consolidate the segmentation results of 3D Gaussians at any training timestamps and conduct the post-processing on this table. For the temporal interpolation task, we adopt the nearest timestamp interpolation in the identity table. Our contribution can be summarized as follows:

- We reformulate the problem of 4D segmentation, and propose the Segment Any 4D Gaussians (SA4D) framework to lift the segment anything model to 4D representation with high efficiency.
- A temporal identity feature field includes a compact network that learns Gaussians’ identity information across time from the noisy feature map input and eases the *Gaussian drifting*. The segmentation refinement process also improves the inference rendering speed and makes scene manipulations simpler and more convenient.
- SA4D achieves fast interactive segmentation within 10 seconds using an RTX 3090 GPU, photo-realistic rendering quality, and enables efficient dynamic scene editing operations seamlessly, e.g. removal, recoloring, and composition.

2 Related Works

3D/4D Representations. Simulating real-world scenes has long been a subject of extensive research in the academic community. Many approaches [19, 20, 21, 22, 23, 24, 25, 26] are proposed to represent real-world scenes and achieve significant success. NeRF [27, 28, 29, 30, 31, 32] and its extensions are proposed to render high-quality novel views even in sparse [33, 34], multi-exposures [35, 36, 37], and show great potential in many downstream tasks [38, 2, 39]. Grid-based representations [40, 41, 42, 43, 44, 45, 46] accelerate NeRF’s training from days into hours even in minutes. Several methods also succeed in modeling dynamic scenes [47, 48, 49, 44, 50] but suffered on volume rendering [51]. Gaussian Splatting (GS) [3, 52, 53, 54] based representations bring rendering speed into real-time while maintaining high training efficiency. Modeling dynamic scenes with Gaussian Splatting exists several ways: incremental translation [55, 56], temporal extension [16, 11, 57] and

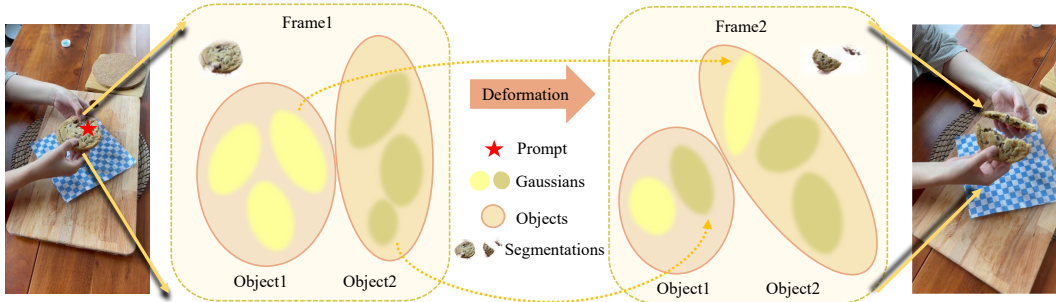


Figure 2: Illustration of *Gaussian drifting* between objects in 4D-GS [15] on the HyperNeRF [18] dataset. The left part is a random input view and the ‘star’ stands for prompt. It is obvious that the segmentation results become inaccurate in different timestamps. It is because some 3D Gaussians of the cookie (object 1) segmented in frame 1 transform into another object (object 2) in frame 2 as shown in the right part.

global deformation [15, 58, 59, 60, 61, 62]. In this paper, we choose the global deformation GS representation, 4D-GS [15], as our 4D representation because it owns a global canonical 3D Gaussians as its geometry and the ability to model monocular/multi-view dynamic scenes. The segmentation results on the deformed 3D Gaussians can also be transformed to the other timestamp easily.

NeRF/Gaussian-based 3D Segmentation. Prior to 3D Gaussians, numerous studies have extended NeRF to 3D scene understanding and segmentation. Semantic-NeRF [63] first incorporated semantic information into NeRF and achieved 3D-consistent semantic segmentation from noisy 2D labels. Then, subsequent researches [64, 65, 66, 67] have developed object-aware implicit representations by introducing instance modeling but relying on GT labels. To achieve open-world scene understanding and segmentation, several approaches [68, 69, 70, 71] distill 2D visual features from 2D foundation models [72, 73, 74] into radiance fields [5, 75]. However, these methods fail to segment semantically similar objects. Therefore, some approaches [2, 76, 6, 4] resorted to SAM’s [1, 6] impressive open-world segmentation capability. The repair process [77] can be followed to extract high-quality object representation after the segmentation process. Nevertheless, all the above methods are constrained to 3D static scenes. However, Directly utilizing the 3D segmentation methods on the 4D representations may also fall to *Gaussian drifting*. Our methods solve the *Gaussian drifting* by maintaining an identity encoding feature field, which models the deformation of semantic information.

Dynamic Scene Segmentation. Few researchers have delved into dynamic scene segmentation. NeuPhysics [78] only allows the complete segmentation of either the dynamic foreground or static background. Recently, 4D-Editor [10] distills DINO features into a hybrid semantic radiance field and conducts 2D-3D feature match and Recursive Selection Refinement method per frame to achieve 4D editing. However, it takes 1-2 seconds to edit one frame. Moreover, ground truth masks of the dynamic foreground are needed to train the hybrid semantic radiance field. These limitations constrain its practical applicability. In this work, we propose a novel 4D segment anything framework enabling efficient dynamic scene editing operations. e.g. recoloring, removal, composition.

3 Preliminaries

3.1 Problem Formulation

Since there are few previous works that mainly focus on 4D segmentation, reformulation is necessary. It is worth noting that the 4D representation shows its weakness in segmentation, we define 4D segmentation as follows:

Problem: Given any deformation-based 4D Gaussian representations O trained on a dataset L , The problem is to find an efficient solution $\mathcal{A} : (O, L) \rightarrow O'$, which O' is a set of object $O' = \{o'_i \mid i = 1, 2, \dots, n\}$. The object o_i should satisfy several features:

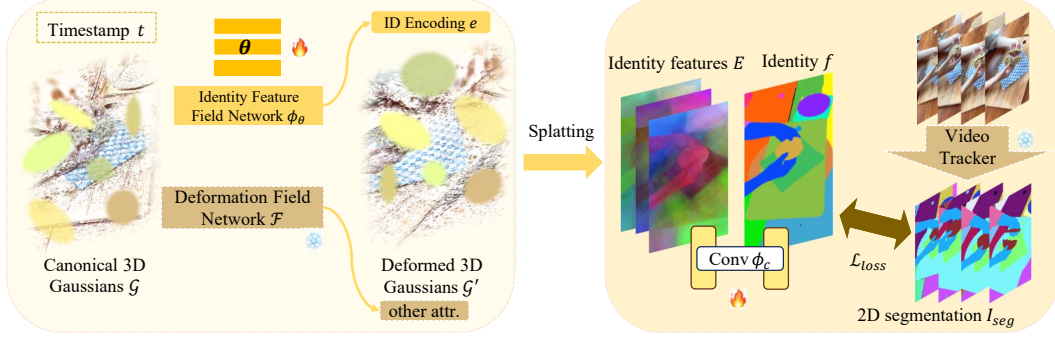


Figure 3: Overview of our training pipeline. Given a timestamp t and canonical 3D Gaussians \mathcal{G} , the ID encoding e and deformed 3D Gaussians \mathcal{G}' will be predicted by an optimizable ϕ_θ and frozen deformation field network \mathcal{F} , respectively. Then the ID encoding e is splatted to E , then ϕ_c is used to classify each pixel's ID f , and the whole training pipeline is supervised by I_{seg} predicted by video tracker with \mathcal{L}_{loss} .

Proposition 1: Given any timestamp t_i , a deformed 3D-GS $\mathcal{G}'_i \in G$ could be export by o_i . e.g:

$$\forall o'_i \in O', \text{export}(o'_i, t_i) \in G. \quad (1)$$

Proposition 2: No ambiguity between all the objects after export in a certain timestamp. e.g:

$$\forall t_i, \{o'_i, o'_j\} \in O', \text{export}(o'_i, t_i) \cap \text{export}(o'_j, t_i) = \emptyset. \quad (2)$$

Proposition 3: Assume there exists a unique real-world 3D object o , then for all $t_i, o'_i \in O'$, we have

$$\forall t_i, o_i \in O', \text{export}(o'_i, t_i) = o. \quad (3)$$

When rasterizing the object o at any views $V = \{M, K\}$, the splatted image of $\hat{I}_{seg} = \mathcal{S}(o, M, K)$ should correspond to ground truth ID segmentation I_{seg} :

$$I_{seg} \sim \hat{I}_{seg} = \mathcal{S}(o, M, K), \quad (4)$$

where \mathcal{S} is differential splatting [79], M is extrinsic matrix and K is camera intrinsic matrix. Because of Eq. (1) and Eq. (3), o can be converted to \hat{I}_{seg} . Finally, we can select any object o'_i by the ID \mathcal{P} from the O' .

3.2 Gaussian Grouping

Gaussian Grouping [6] extends Gaussian Splatting to jointly reconstruct and segment anything in open-world 3D scenes. It introduces to each Gaussian a new parameter, identity encoding, to group and segment anything in 3D-GS [3]. These identity encodings e are then attached to the 3D Gaussians along with other attributes. Similar to rendering the RGB image in [3], 3D Gaussians to a specific camera view and compute the 2D identity feature E_{id} of a pixel p by differential splatting algorithm [79] \mathcal{S} :

$$E_p = \mathcal{S}(\mathcal{G}, M, K) = \sum_{i \in \mathcal{N}} e_i \alpha_i \prod_{j=1}^{i-1} (1 - \alpha_j), \quad (5)$$

where e_i, α_i represents the Identity Encoding and density of the i -th Gaussian under the view $\{M, K\}$. In [6], a linear classifier f segments the rendered image, which takes the rendered 2D identity feature map E as inputs. Since 3D segmentation can be considered as a 4D scene with only one timestamp, **proposition 1,2,3** are also satisfied.

3.3 4D Gaussian Splatting

4D Gaussian Splatting (4D-GS) [15] extends 3D-GS [3] to model dynamic scenes efficiently, which represent 4D scene by a compact representation $O = \{\mathcal{G}, \mathcal{F}_\theta(\mathcal{G}, t)\}$. $\mathcal{G} \in G$ is a set of canonical 3D

Gaussians belongs to 3D-GS \mathcal{G} and the Gaussian deformation field network \mathcal{F} contains a spatial-temporal structure encoder \mathcal{H} and a multi-head Gaussian deformation decoder \mathcal{D} . At timestamp t , the temporal and spatial features of 3D Gaussians are encoded through the spatial-temporal structure encoder:

$$f_d = \mathcal{H}(\mathcal{G}, t). \quad (6)$$

Then, the deformation decoder $\mathcal{D} = \{\phi_x, \phi_r, \phi_s\}$ employs three separate MLPs to compute the deformation of Gaussians’ position, rotation, and scaling:

$$(\Delta\mathcal{X}, \Delta r, \Delta s) = \mathcal{D}(f_d) = (\phi_x(f_d), \phi_r(f_d), \phi_s(f_d)). \quad (7)$$

Finally, we can *export* the deformed 3D Gaussians $\mathcal{G}' = \{\mathcal{X}', r', s', \sigma, \mathcal{C}\} = \{\mathcal{X} + \Delta\mathcal{X}, r + \Delta r, s + \Delta s, \sigma, \mathcal{C}\}$ and render novel views $I = \mathcal{S}(\mathcal{G}', M, K)$ via differential splatting \mathcal{S} [79] given any camera poses. To this end, we define the *export* process of 4D-GS as:

$$\mathcal{G}'_i = \text{export}(O, t_i) = \mathcal{F}(\mathcal{G}, t_i), \quad (8)$$

which could satisfy the Eq. (3). It means that \mathcal{G} are mapped to \mathcal{G}'_i conditioned on t_i by \mathcal{F} . However, when conducting 4D segmentation, the vanilla 4D-GS pipeline doesn’t contain any 4D semantic information. Though canonical 3D Gaussians can be divided into a subset of 3D Gaussians \mathcal{G}_i if adding e_i to g_i directly, which can satisfy the **proposition 1,2**, both canonical 3D Gaussians \mathcal{G}_i and deformation field network \mathcal{F} cannot identify each object and cause *Gaussian drifting* as shown in Fig. 2. Therefore, the **proposition 3** is hard to be served. To address the problem, our SA4D framework is introduced.

4 SA4D

4.1 Overall Framework

Our key insight is introducing a representation to encode the temporal semantic information from a pretrained foundation model \mathcal{V} to help the *export* process since conduct segmentation in 4D-GS cannot afford the **proposition 3**. In SA4D, we refine the *export* process as follows:

$$\mathcal{G}'_i = \text{export}(o_i, t_i) = \mathcal{F}_\theta(\mathcal{G}_i, t_i) \cap \mathcal{F}(\mathcal{G}, t_i), \quad (9)$$

where \mathcal{F}_θ is our proposed SA4D representation including a temporal identity feature field ϕ_θ , tiny convolutional decoder ϕ_c and a Gaussian identity table \mathcal{M} as shown in Eq. (10):

$$\mathcal{F}_\theta = f \cap M_i(f, I_{mask}, t_i), \quad (10)$$

in which f is the Gaussian identity which is predicted by the identity encoding feature field as it is discussed in Sec 4.2, the latter is the post-process formula in Sec 4.3.

4.2 Identity Encoding Feature Field

Temporal Identity Feature Field Network. To address the challenges of *Gaussian drifting* discussed in Sec. 1, we propose an identity feature field network \mathcal{F}_θ to encode identity features at each timestamp. Given time t and center position \mathcal{X} of 3D Gaussians \mathcal{G} in the canonical space as inputs, the temporal identity feature field network predicts a low-dimensional time-variant Identity features e for each Gaussian:

$$e = \phi_\theta(\gamma(\mathcal{X}), \gamma(t)), \quad (11)$$

where θ denotes the learnable parameters of the network and γ denotes the positional encoding [80]. Then, identity splatting as shown in Eq. (5) is rendered to get E_p . Note that the supervision is the identity of each pixel, we use a tiny convolutional decoder ϕ_c and the softmax function to predict Gaussian identity f as shown in Eq. (12):

$$f = \text{softmax}(\phi_c(E_p)). \quad (12)$$

Optimization. Since it is hard to access GT 4D object labels, we cannot supervise the training process with o . Therefore, we adopt the 2D pseudo segmentation results of foundation video tracker I_{mask} as the supervision. Similar to [6], we use the 2D Identity Loss L_{2d} and 3D Regularization

Loss L_{3d} to supervise the training process $L = \lambda_{2d}L_{2d} + \lambda_{3d}L_{3d}$. Identity loss L_{2d} is a standard cross-entropy loss on the training image I :

$$L_{2d} = -\frac{1}{||I||} \sum_{i \in I} \sum_{c=1}^C p(i) \log \hat{p}(i), \quad (13)$$

where C is the total number of mask identities in I_{mask} and p and \hat{p} are the multi-identity probability of gt mask I_{mask} and our network predictions. 3D Regularization Loss L_{3d} in [6] is applied to further supervise the Gaussians inside 3D objects and heavily occluded. It is the KL divergence loss, enforcing the Identity Encodings of the top k -nearest 3D Gaussians to be close in their feature distance:

$$L_{3d} = \frac{1}{m} \sum_{j=1}^m D_{KL}(P||Q) = \frac{1}{mk} \sum_{j=1}^m \sum_{i=1}^k f_j \log \frac{f_j}{f_i}, \quad (14)$$

where m is the number of sampled Gaussians, P is the j -th Gaussian and Q is the set of its k -nearest neighbors in the deformed space.

4.3 4D Segmentation Refinement

Post Processing. Though the temporal identity feature field network shows the ability to encode temporal identity features of 3D Gaussians, the *export* process is still affected by the heavily occluded and invisible Gaussians and the noisy segmentation supervision. To get a more precise \mathcal{G}'_i which is similar to o , we employ 2-step post-processing. The first step is removing outliers, the same as [4, 6]. However, there are still some ambiguous Gaussians at the interface between two objects, as discussed in [2], which do not or slightly affect the quantitative results but impair the geometry correctness of the segmentation target o' . Therefore, in the second step, similar to [2], we utilize the 2D segmentation supervision I_{mask} as prior to eliminate these ambiguous Gaussians. Concretely, we assign each Gaussian g a mask $m = \mathbb{I}(g \in o')$, render 3D point masks and apply the mask projection loss in [2]:

$$L_{proj} = -\sum_{i \in I} M_{o'}(i) \cdot M(i) + \lambda \sum_{i \in I} (1 - M_{o'}(i)) \cdot M(i), \quad (15)$$

where $M_{o'}$ denotes the mask of o' in I_{mask} , M is the rendered object mask and λ is a hyper-parameter to determine the magnitude of the negative term. The Gaussians with negative gradients are then removed. The greater λ is, the more sensitive L_{proj} is to the ambiguous Gaussians.

Gaussian Identity Table. Going through the implicit identity encoding field network and performing post-process frame-by-frame during inference are time-consuming and inconvenient for scene editing. Therefore, we propose to store the segmentation results at each training timestamp in a Gaussian identity table \mathcal{M} and employ the nearest timestamp interpolation *nearest* during inference as shown in Eq. (16):

$$M_i = \text{nearest}(\mathcal{M}(g, t_i)). \quad (16)$$

Concretely, after training, users can input an object ID. Our method segments out 4D Gaussians that belong to the object at each training timestamp according to their Identity Encoding. The final segmentation results are stored in the Gaussian identity table. The post-process procedure can be applied in the \mathcal{M} before rendering. This process can be finished within 10 seconds in most cases and increase the rendering speed during inference significantly. The details of the 4D segmentation refinement are in Algorithm. 2.

5 Experiment

5.1 Experimental setups

Implementation Details. Our implementation is primarily based on the PyTorch [82] framework and tested in a single RTX 3090 GPU. For simplicity, we train our framework based on a pre-trained 4D-GS [15]. The output dimension of the temporal identity feature field network, e.g. Identity Encoding dimension, is set to 32. The classification convolutional layer has 32 input channels and 256 output channels. We use the Adam optimizer for both the temporal identity feature field network

Method	HyperNeRF [18]		Neu3D [81]	
	mIoU(%)	mAcc(%)	mIoU(%)	mAcc(%)
SAGA [4]	65.25	75.56	76.26	81.56
Gaussian Grouping [6]	69.53	91.55	87.02	98.72
Ours w/o TFF (w/o Refinement)	80.26	99.56	-	-
Ours w/ TFF (w/o Refinement)	81.10	99.54	80.14	99.88
Ours w/ all	89.86	99.24	93.02	99.76

Table 1: Evaluation metrics on the HyperNeRF [18] and Neu3D [81] dataset. ‘‘Ours w/o TFF’’ means directly attaching an identity feature vector to each Gaussian.

and convolutional layer, with 5000 training iterations and a learning rate of $5e - 4$. The training process costs about half an hour for a standard scene with 200k Gaussians under the resolution of 1352×1014 . For optimization loss, we choose $\lambda_{2d} = 1$, $\lambda_{3d} = 2$, $k = 5$, and $m = 1000$, the same as [6]. Note that we only use images under one camera as training inputs for Neu3D [83] scenes because of the ID conflict problem produced by [17]. We leave the problem as our future work.

Datasets. We use two widely-used dynamic scene datasets in our experiments, which are HyperNeRF dataset [18] and Neu3D dataset [81]. As there are no ground truth segmentation mask labels for these datasets, we annotate some dynamic objects in test views in these scenes for our evaluation. Details about mask annotation are provided in the Supp. file.

Baselines. Due to the lack of open source code for [10] and no other 4D segmentation methods, we choose 3D segmentation methods as our baselines. Most recent Gaussian-based 3D segmentation methods also lack open source code and Feature-3DGS [5] mainly focuses on semantic segmentation and language-driven editing, so we choose SAGA [4] and Gaussian Grouping [6] for comparison. Since they do not have the temporal dimension and are limited to 3D static scenes, we conduct training and segmentation on a certain training timestamp based on the **deformed 3D Gaussians** in 4D-GS [15]. The segmentation results are then propagated to other timestamps and viewed through 4D-GS’s deformation field. We train the baseline models on 10 randomly selected timestamps separately for each scene and reported the average test results.

5.2 Results

Since acquiring and annotating 3D/4D Gaussian labels is significantly challenging, we render 3D point masks to 2D, threshold the rendered 2D mask value to be greater than 0.1 to remove the low-density areas that contribute negligibly to the rendered visuals and calculate the IoU and Accuracy. The averaged quantitative results are provided in Tab. 1 and per-scene results are provided in Tab. 4 and Tab. 5. Visual comparisons are shown in Fig. 4 and more visualization results are provided in Fig. 9, Fig. 10 and Fig. 11. The quantitative results on HyperNeRF [18] scenes are shown in Tab. 4. In the monocular setting, existing 3D segmentation methods can only rely on one view at one timestamp rather than multi-view observations. Therefore, the two baselines produce terrible segmentation results. The reason that the Gaussian Grouping baseline has low mIoU but high mACC is that it incorporates too much noise due to the heavy occlusion and monocular sparsity during training. The baselines also suffer from the *Gaussian Drifting* problem as shown in the *split-cookie* scene in Fig. 4. Although 3D segmentation models [4] [6] successfully segment out the 3D Gaussians of the cookie at the first frame and track their motions, one piece of the cookie disappears later. In contrast, our method can accurately identify the 3D Gaussians belonging to the cookie at different timestamps remedying the *Gaussian Drifting* problem.

The quantitative results on Neu3D scenes are shown in Tab. 5. The Neu3D datasets are less challenging than the monocular datasets because 4D-GS [15] can model the motion more accurately in the multi-view setting and 3D segmentation models have multi-view observations at one timestamp. Also, the *Gaussian Drifting* problem is not obvious. However, our method still has superior performance

Model	FPS	Storage(MB)
Ours w/o. GIT	7.12	62.55
Ours	40.36	80.12

Table 2: Ablation of the Gaussian Identity Table.

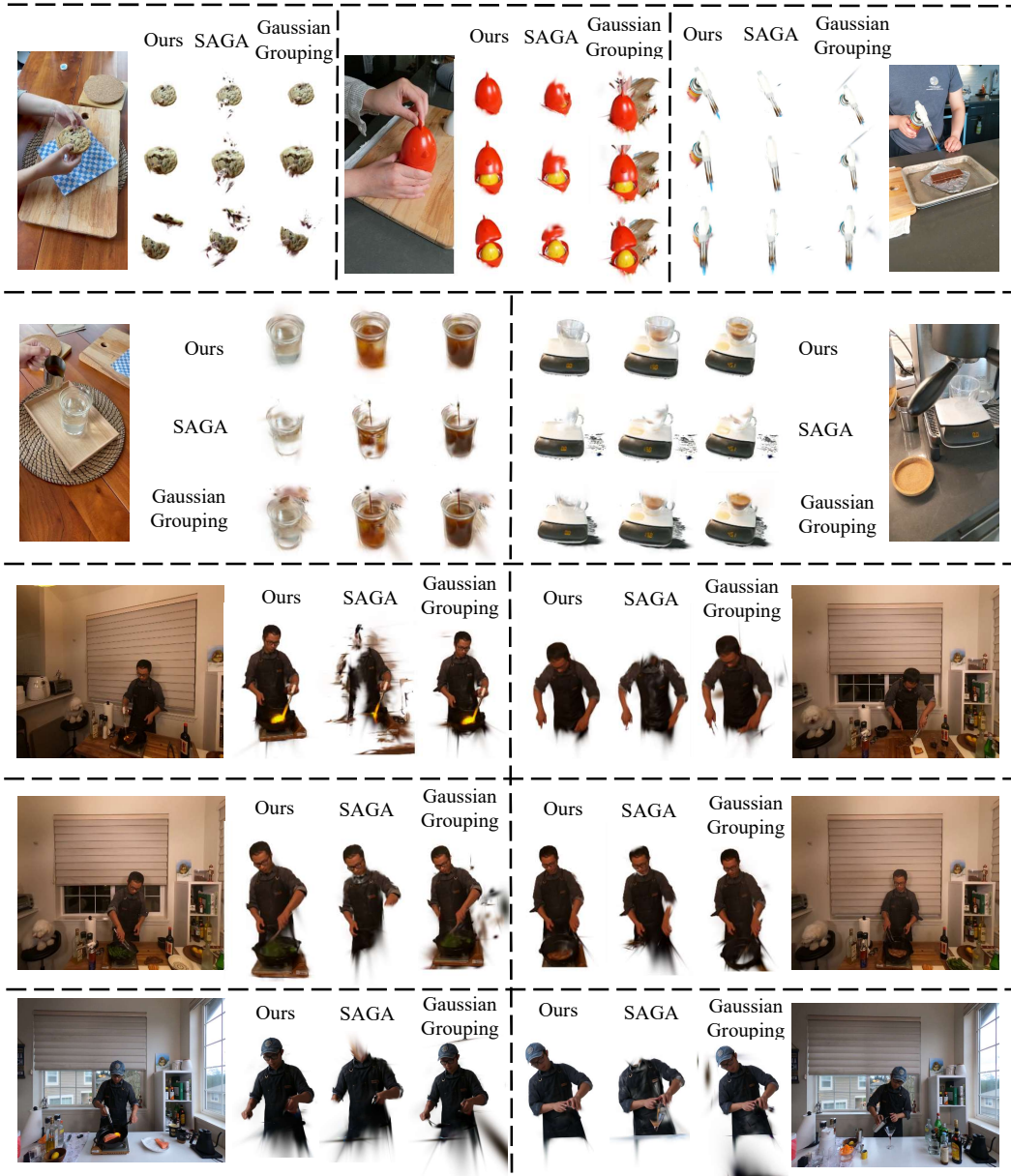


Figure 4: Visual comparisons of our method and baselines on the HyperNeRF [18] and Neu3D [81] dataset. The upper five scenes are from the HyperNeRF dataset and we visualize and compare the segmentation results at three random novel views and timestamps for each scene. The lower six scenes are from the Neu3D dataset and we visualize and compare the segmentation results at one random novel view and timestamp for each scene.

over the two baselines by learning temporal identity features. SAGA [4]’s performance is not stable because it is class-agnostic and it struggles to segment large objects with multiple semantics. Utilizing multi-view information, Gaussian Grouping [6] sometimes outperforms ours w/o refinement. Note that since we only train our model with temporal mask identities in a single view, the initial segmentation results before refinement are sometimes noisy.

5.3 Dynamic Scene Editing

In Fig. 1 and Fig. 5, we show some applications of our SA4D framework. Thanks to the explicitness of the 4D Gaussian representation and our Gaussian identity table, we can retrieve the 3D Gaussians of



Figure 5: More examples of composition, deletion with segmented 4D Gaussians. (a): copying a cookie in the scene. (b) Deleting the cup in the scene. (c) Compositing the man with a room in Neu3D [83] and Mip-NeRF360 [84] dataset. (d) Compositing the chickchicken with the man in HyperNeRF [18] and Neu3D [83] dataset.

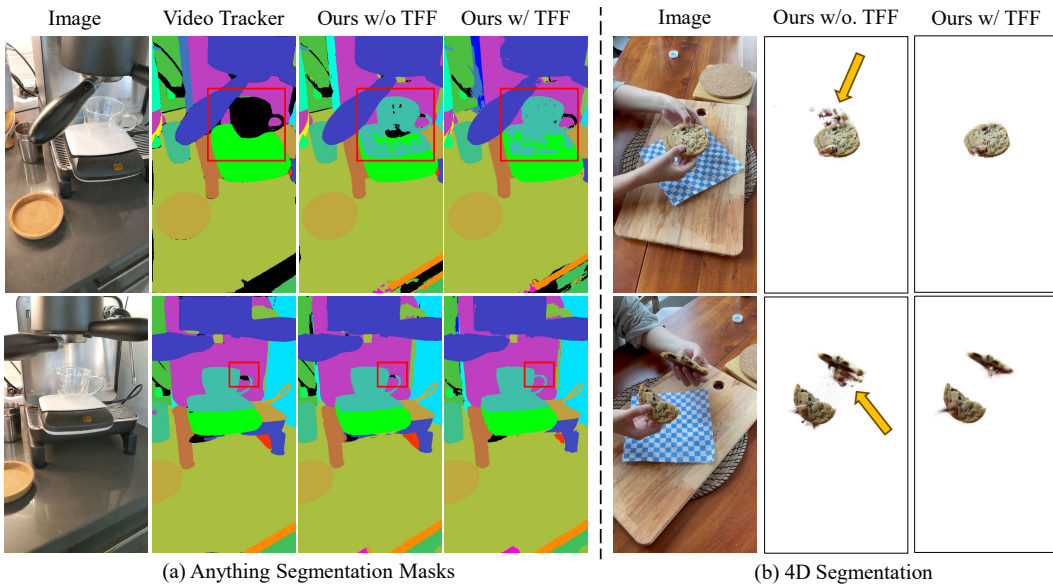


Figure 6: Ablation study of our temporal identity field network. (a) The black regions represent the void class (Illustrated as black color). Predictions from input 2D supervision (e.g. video tracker [17]) are sometimes incorrect (e.g. cup labeled void 0 in the image above) and noisy (e.g. handle labeled void in the image below). (b) Due to the *Gaussian drifting*, some Gaussians outside the cookie in the image above will transform into the cookie as shown in the image below.

an object at each timestamp in real time and then manipulate them easily and quickly. For example, the object can be copied in the 4D scene as shown in column (a) of Fig. 5, removed as shown in column (b), composited with 3D Gaussians as shown in column (c) or composited with other 4D Gaussians in column (d).

5.4 Ablation Study

Temporal Identity Feature Field Network. Instead of attaching a time-invariant feature vector to each Gaussian as most 3D segmentation methods do, we introduce a Temporal Identity Feature Field Network (TFF) to encode identity features across time to solve the Gaussian drifting. We compare the two methods on monocular datasets, HyperNeRF [18], where it is challenging for 4D-GS [15] to model motion accurately. Note that we did not conduct post-processing in our ablation study of TFF in order to study the effect of Gaussian drifting. As shown in Tab. 4, ours w/ TFF outperforms ours w/o TFF on most scenes, especially on the split-cookie scene where we observe severe Gaussian drifting. We also found that our temporal identity field shows the ability to learn accurate ID information from noisy input 2D segmentation supervision. Visual comparisons and illustrations are shown in Fig. 6.

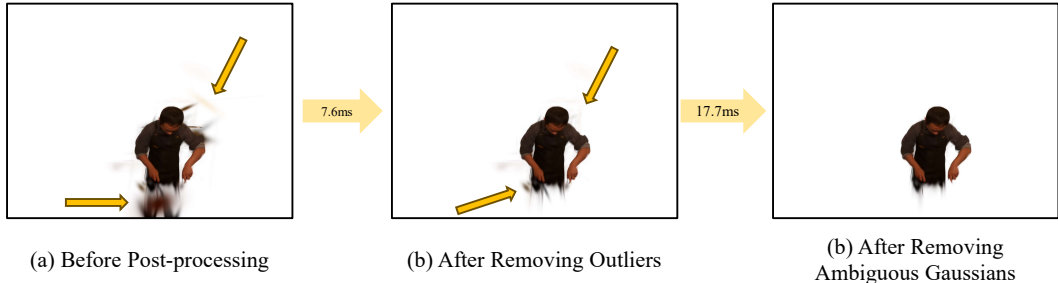


Figure 7: Ablation study on the effect of the post-processing in 4D segmentation refinement. Time in the arrows stands for the average time consumption in each frame.

4D Segmentation Refinement. Since the segmentation supervision is in 2D, the initial segmentation result is typically noisy, including artifacts far away from the object and ambiguous Gaussians at the boundary fitting the color of multiple objects. As shown in Tab. 1 and Fig. 7, our refinement approach can obviously improve the segmentation quality and eliminate artifacts and ambiguous Gaussians at the boundary. Note that ambiguous Gaussians at the boundary partially overlap with the object, so removing them may result in a slight decrease in segmentation accuracy. We conduct ablation studies on the ‘split-cookie’ in the HyperNeRF [18] dataset. Tab. 2 shows that the Gaussian Identity Table we proposed can maintain the real-time rendering speed of 4D-GS while not increasing too much storage. We also study the effect of the timestamp interval in 4D segmentation refinement. Tab. 3 shows that with the interval increasing, although the refinement time decreases, the segmentation quality downgrades.

Interval	Time(s)	IoU(%)	Acc(%)
1	7.8	88.92	99.73
2	3.91	88.91	99.74
4	1.82	88.61	99.66
8	0.90	88.11	99.51
16	0.48	87.58	99.07

Table 3: Ablation on refinement interval. ‘Time’ in the table represents the time cost by 4D segmentation refinement.

6 Limitation

Though SA4D can achieve fast and high-quality segmentation in 4D Gaussians, some limitations exist and can be explored in future works. (1) Similar to Gaussian Grouping [6], selecting an object needs an identity number as prompt, which causes difficulty for selecting desired object comparing with ‘click’ or language. (2) The deformation field cannot be decomposed at the object level, necessitating the involvement of the entire deformation network in the segmentation and rendering process. (3) The mask identity conflicts between different video inputs make it difficult to utilize multi-view information effectively. (4) Similar to 3D segmentation, object artifacts still exist due to the features of 3D Gaussians.

7 Conclusion

This paper proposes a Segment Any 4D Gaussians framework to achieve fast and precise segmentation in 4D-GS [15]. The semantic supervision from world space in different timestamps is converted to canonical space by the 4D-GS and temporal identity feature field network. The temporal identity feature field network also solves the *Gaussian drifting* problem. SA4D can render high-quality novel view segmentation results and also supports some editing tasks, such as object removal, composition, and recoloring.

References

- [1] Alexander Kirillov, Eric Mintun, Nikhila Ravi, Hanzi Mao, Chloe Rolland, Laura Gustafson, Tete Xiao, Spencer Whitehead, Alexander C Berg, Wan-Yen Lo, et al. Segment anything. In *Proceedings of the IEEE/CVF International Conference on Computer Vision*, pages 4015–4026, 2023.
- [2] Jiazong Cen, Zanwei Zhou, Jiemin Fang, Wei Shen, Lingxi Xie, Xiaopeng Zhang, and Qi Tian. Segment anything in 3d with nerfs. In *NeurIPS*, 2023.
- [3] Bernhard Kerbl, Georgios Kopanas, Thomas Leimkühler, and George Drettakis. 3d gaussian splatting for real-time radiance field rendering. *ACM Transactions on Graphics (ToG)*, 42(4):1–14, 2023.

- [4] Jiazhong Cen, Jiemin Fang, Chen Yang, Lingxi Xie, Xiaopeng Zhang, Wei Shen, and Qi Tian. Segment any 3d gaussians. *arXiv preprint arXiv:2312.00860*, 2023.
- [5] Shijie Zhou, Haoran Chang, Sicheng Jiang, Zhiwen Fan, Zehao Zhu, Dejia Xu, Pradyumna Chari, Suya You, Zhangyang Wang, and Achuta Kadambi. Feature 3dgs: Supercharging 3d gaussian splatting to enable distilled feature fields. 2024.
- [6] Mingqiao Ye, Martin Danelljan, Fisher Yu, and Lei Ke. Gaussian grouping: Segment and edit anything in 3d scenes. *arXiv preprint arXiv:2312.00732*, 2023.
- [7] Chen Gao, Ayush Saraf, Johannes Kopf, and Jia-Bin Huang. Dynamic view synthesis from dynamic monocular video. In *Proceedings of the IEEE/CVF International Conference on Computer Vision*, pages 5712–5721, 2021.
- [8] Fengrui Tian, Shaoyi Du, and Yueqi Duan. Mononerf: Learning a generalizable dynamic radiance field from monocular videos. In *Proceedings of the IEEE/CVF International Conference on Computer Vision*, pages 17903–17913, 2023.
- [9] Yu-Lun Liu, Chen Gao, Andreas Meuleman, Hung-Yu Tseng, Ayush Saraf, Changil Kim, Yung-Yu Chuang, Johannes Kopf, and Jia-Bin Huang. Robust dynamic radiance fields. In *Proceedings of the IEEE/CVF Conference on Computer Vision and Pattern Recognition*, pages 13–23, 2023.
- [10] Dadong Jiang, Zhihui Ke, Xiaobo Zhou, and Xidong Shi. 4d-editor: Interactive object-level editing in dynamic neural radiance fields via 4d semantic segmentation. *arXiv preprint arXiv:2310.16858*, 2023.
- [11] Zeyu Yang, Hongye Yang, Zijie Pan, Xiatian Zhu, and Li Zhang. Real-time photorealistic dynamic scene representation and rendering with 4d gaussian splatting. 2024.
- [12] Yurui Chen, Chun Gu, Junzhe Jiang, Xiatian Zhu, and Li Zhang. Periodic vibration gaussian: Dynamic urban scene reconstruction and real-time rendering. *arXiv preprint arXiv:2311.18561*, 2023.
- [13] Yunzhi Yan, Haotong Lin, Chenxu Zhou, Weijie Wang, Haiyang Sun, Kun Zhan, Xianpeng Lang, Xiaowei Zhou, and Sida Peng. Street gaussians for modeling dynamic urban scenes. *arXiv preprint arXiv:2401.01339*, 2024.
- [14] Xu Hu, Yuxi Wang, Lue Fan, Junsong Fan, Junran Peng, Zhen Lei, Qing Li, and Zhaoxiang Zhang. Segment anything in 3d gaussians, 2024.
- [15] Guanjun Wu, Taoran Yi, Jiemin Fang, Lingxi Xie, Xiaopeng Zhang, Wei Wei, Wenyu Liu, Qi Tian, and Xinggang Wang. 4d gaussian splatting for real-time dynamic scene rendering. 2024.
- [16] Yuanxing Duan, Fangyin Wei, Qiyu Dai, Yuhang He, Wenzheng Chen, and Baoquan Chen. 4d gaussian splatting: Towards efficient novel view synthesis for dynamic scenes. *arXiv preprint arXiv:2402.03307*, 2024.
- [17] H. Cheng, S. Wug Oh, B. Price, A. Schwing, and J. Lee. Tracking anything with decoupled video segmentation. In *2023 IEEE/CVF International Conference on Computer Vision (ICCV)*, pages 1316–1326, Los Alamitos, CA, USA, oct 2023. IEEE Computer Society.
- [18] Keunhong Park, Utkarsh Sinha, Peter Hedman, Jonathan T Barron, Sofien Bouaziz, Dan B Goldman, Ricardo Martin-Brualla, and Steven M Seitz. Hypernerf: A higher-dimensional representation for topologically varying neural radiance fields. *arXiv preprint arXiv:2106.13228*, 2021.
- [19] Alvaro Collet, Ming Chuang, Pat Sweeney, Don Gillett, Dennis Evseev, David Calabrese, Hugues Hoppe, Adam Kirk, and Steve Sullivan. High-quality streamable free-viewpoint video. *ACM Transactions on Graphics (ToG)*, 34(4):1–13, 2015.
- [20] Zhong Li, Minye Wu, Wangyiteng Zhou, and Jingyi Yu. 4d human body correspondences from panoramic depth maps. In *Proceedings of the IEEE Conference on Computer Vision and Pattern Recognition*, pages 2877–2886, 2018.
- [21] Kaiwen Guo, Feng Xu, Yangang Wang, Yebin Liu, and Qionghai Dai. Robust non-rigid motion tracking and surface reconstruction using l0 regularization. In *Proceedings of the IEEE International Conference on Computer Vision*, pages 3083–3091, 2015.
- [22] Zhuo Su, Lan Xu, Zerong Zheng, Tao Yu, Yebin Liu, and Lu Fang. Robustfusion: Human volumetric capture with data-driven visual cues using a rgbd camera. In *Computer Vision–ECCV 2020: 16th European Conference, Glasgow, UK, August 23–28, 2020, Proceedings, Part IV 16*, pages 246–264. Springer, 2020.
- [23] John Flynn, Michael Broxton, Paul Debevec, Matthew DuVall, Graham Fyffe, Ryan Overbeck, Noah Snavely, and Richard Tucker. Deepview: View synthesis with learned gradient descent. In *Proceedings of the IEEE/CVF Conference on Computer Vision and Pattern Recognition*, pages 2367–2376, 2019.
- [24] Kaiwen Guo, Peter Lincoln, Philip Davidson, Jay Busch, Xueming Yu, Matt Whalen, Geoff Harvey, Sergio Orts-Escolano, Rohit Pandey, Jason Dourgarian, et al. The relightables: Volumetric performance capture of humans with realistic relighting. *ACM Transactions on Graphics (ToG)*, 38(6):1–19, 2019.

- [25] Tao Hu, Tao Yu, Zerong Zheng, He Zhang, Yebin Liu, and Matthias Zwicker. Hivr: Hybrid volumetric-textural rendering for human avatars. In *2022 International Conference on 3D Vision (3DV)*, pages 197–208. IEEE, 2022.
- [26] Zhong Li, Yu Ji, Wei Yang, Jinwei Ye, and Jingyi Yu. Robust 3d human motion reconstruction via dynamic template construction. In *2017 International Conference on 3D Vision (3DV)*, pages 496–505. IEEE, 2017.
- [27] Ben Mildenhall, Pratul P Srinivasan, Matthew Tancik, Jonathan T Barron, Ravi Ramamoorthi, and Ren Ng. Nerf: Representing scenes as neural radiance fields for view synthesis. *Communications of the ACM*, 65(1):99–106, 2021.
- [28] Jonathan T Barron, Ben Mildenhall, Matthew Tancik, Peter Hedman, Ricardo Martin-Brualla, and Pratul P Srinivasan. Mip-nerf: A multiscale representation for anti-aliasing neural radiance fields. In *Proceedings of the IEEE/CVF International Conference on Computer Vision*, pages 5855–5864, 2021.
- [29] Kai Zhang, Gernot Riegler, Noah Snaveley, and Vladlen Koltun. Nerf++: Analyzing and improving neural radiance fields. *arXiv preprint arXiv:2010.07492*, 2020.
- [30] Yiming Wang, Qin Han, Marc Habermann, Kostas Daniilidis, Christian Theobalt, and Lingjie Liu. Neus2: Fast learning of neural implicit surfaces for multi-view reconstruction. In *Proceedings of the IEEE/CVF International Conference on Computer Vision*, pages 3295–3306, 2023.
- [31] Mateusz Michalkiewicz, Jhony K Pontes, Dominic Jack, Mahsa Baktashmotlagh, and Anders Eriksson. Implicit surface representations as layers in neural networks. In *Proceedings of the IEEE/CVF International Conference on Computer Vision*, pages 4743–4752, 2019.
- [32] Licheng Zhong, Lixin Yang, Kailin Li, Haoyu Zhen, Mei Han, and Cewu Lu. Color-neus: Reconstructing neural implicit surfaces with color. 2024.
- [33] Ruoshi Liu, Rundi Wu, Basile Van Hoorick, Pavel Tokmakov, Sergey Zakharov, and Carl Vondrick. Zero-1-to-3: Zero-shot one image to 3d object. In *Proceedings of the IEEE/CVF International Conference on Computer Vision*, pages 9298–9309, 2023.
- [34] Yabo Chen, Jiemin Fang, Yuyang Huang, Taoran Yi, Xiaopeng Zhang, Lingxi Xie, Xinggang Wang, Wenrui Dai, Hongkai Xiong, and Qi Tian. Cascade-zero123: One image to highly consistent 3d with self-prompted nearby views. *arXiv preprint arXiv:2312.04424*, 2023.
- [35] Ricardo Martin-Brualla, Noha Radwan, Mehdi SM Sajjadi, Jonathan T Barron, Alexey Dosovitskiy, and Daniel Duckworth. Nerf in the wild: Neural radiance fields for unconstrained photo collections. In *Proceedings of the IEEE/CVF Conference on Computer Vision and Pattern Recognition*, pages 7210–7219, 2021.
- [36] Xin Huang, Qi Zhang, Ying Feng, Hongdong Li, Xuan Wang, and Qing Wang. Hdr-nerf: High dynamic range neural radiance fields. In *Proceedings of the IEEE/CVF Conference on Computer Vision and Pattern Recognition*, pages 18398–18408, 2022.
- [37] Guanjun Wu, Taoran Yi, Jiemin Fang, Wenyu Liu, and Xinggang Wang. Fast high dynamic range radiance fields for dynamic scenes. 2024.
- [38] Yu-Jie Yuan, Yang-Tian Sun, Yu-Kun Lai, Yuewen Ma, Rongfei Jia, and Lin Gao. Nerf-editing: geometry editing of neural radiance fields. In *Proceedings of the IEEE/CVF Conference on Computer Vision and Pattern Recognition*, pages 18353–18364, 2022.
- [39] Ben Poole, Ajay Jain, Jonathan T Barron, and Ben Mildenhall. Dreamfusion: Text-to-3d using 2d diffusion. *arXiv preprint arXiv:2209.14988*, 2022.
- [40] Cheng Sun, Min Sun, and Hwann-Tzong Chen. Direct voxel grid optimization: Super-fast convergence for radiance fields reconstruction. In *Proceedings of the IEEE/CVF Conference on Computer Vision and Pattern Recognition*, pages 5459–5469, 2022.
- [41] Sara Fridovich-Keil, Alex Yu, Matthew Tancik, Qinhong Chen, Benjamin Recht, and Angjoo Kanazawa. Plenoxels: Radiance fields without neural networks. In *Proceedings of the IEEE/CVF Conference on Computer Vision and Pattern Recognition*, pages 5501–5510, 2022.
- [42] Zhen Xu, Sida Peng, Haotong Lin, Guangzhao He, Jiaming Sun, Yujun Shen, Hujun Bao, and Xiaowei Zhou. 4k4d: Real-time 4d view synthesis at 4k resolution. 2023.
- [43] Taoran Yi, Jiemin Fang, Xinggang Wang, and Wenyu Liu. Generalizable neural voxels for fast human radiance fields. *arXiv preprint arXiv:2303.15387*, 2023.
- [44] Ruizhi Shao, Zerong Zheng, Hanzhang Tu, Boning Liu, Hongwen Zhang, and Yebin Liu. Tensor4d: Efficient neural 4d decomposition for high-fidelity dynamic reconstruction and rendering. In *Proceedings of the IEEE/CVF Conference on Computer Vision and Pattern Recognition*, pages 16632–16642, 2023.
- [45] Wanshui Gan, Hongbin Xu, Yi Huang, Shifeng Chen, and Naoto Yokoya. V4d: Voxel for 4d novel view synthesis. *IEEE Transactions on Visualization and Computer Graphics*, 2023.

- [46] Feng Wang, Zilong Chen, Guokang Wang, Yafei Song, and Huaping Liu. Masked space-time hash encoding for efficient dynamic scene reconstruction. *Advances in neural information processing systems*, 2023.
- [47] Jiemin Fang, Taoran Yi, Xinggang Wang, Lingxi Xie, Xiaopeng Zhang, Wenyu Liu, Matthias Nießner, and Qi Tian. Fast dynamic radiance fields with time-aware neural voxels. In *SIGGRAPH Asia 2022 Conference Papers*, pages 1–9, 2022.
- [48] Ang Cao and Justin Johnson. Hexplane: A fast representation for dynamic scenes. In *Proceedings of the IEEE/CVF Conference on Computer Vision and Pattern Recognition*, pages 130–141, 2023.
- [49] Sara Fridovich-Keil, Giacomo Meanti, Frederik Rahbæk Warburg, Benjamin Recht, and Angjoo Kanazawa. K-planes: Explicit radiance fields in space, time, and appearance. In *Proceedings of the IEEE/CVF Conference on Computer Vision and Pattern Recognition*, pages 12479–12488, 2023.
- [50] Haotong Lin, Sida Peng, Zhen Xu, Tao Xie, Xingyi He, Hujun Bao, and Xiaowei Zhou. High-fidelity and real-time novel view synthesis for dynamic scenes. In *SIGGRAPH Asia Conference Proceedings*, 2023.
- [51] Robert A Drebin, Loren Carpenter, and Pat Hanrahan. Volume rendering. *ACM Siggraph Computer Graphics*, 22(4):65–74, 1988.
- [52] Binbin Huang, Zehao Yu, Anpei Chen, Andreas Geiger, and Shenghua Gao. 2d gaussian splatting for geometrically accurate radiance fields. *arXiv preprint arXiv:2403.17888*, 2024.
- [53] Zehao Yu, Anpei Chen, Binbin Huang, Torsten Sattler, and Andreas Geiger. Mip-splatting: Alias-free 3d gaussian splatting. *arXiv preprint arXiv:2311.16493*, 2023.
- [54] Yuyang Yin, Dejia Xu, Zhangyang Wang, Yao Zhao, and Yunchao Wei. 4dgen: Grounded 4d content generation with spatial-temporal consistency. *arXiv preprint arXiv:2312.17225*, 2023.
- [55] Jonathon Luiten, Georgios Kopanas, Bastian Leibe, and Deva Ramanan. Dynamic 3d gaussians: Tracking by persistent dynamic view synthesis. In *3DV*, 2024.
- [56] Jiakai Sun, Han Jiao, Guangyuan Li, Zhanjie Zhang, Lei Zhao, and Wei Xing. 3dstream: On-the-fly training of 3d gaussians for efficient streaming of photo-realistic free-viewpoint videos. 2024.
- [57] Shuai Zhang, Huangxuan Zhao, Zhenghong Zhou, Guanjun Wu, Chuansheng Zheng, Xinggang Wang, and Wenyu Liu. Togs: Gaussian splatting with temporal opacity offset for real-time 4d dsa rendering. *arXiv preprint arXiv:2403.19586*, 2024.
- [58] Ziyi Yang, Xinyu Gao, Wen Zhou, Shaohui Jiao, Yuqing Zhang, and Xiaogang Jin. Deformable 3d gaussians for high-fidelity monocular dynamic scene reconstruction. 2024.
- [59] Yi-Hua Huang, Yang-Tian Sun, Ziyi Yang, Xiaoyang Lyu, Yan-Pei Cao, and Xiaojuan Qi. Sc-gs: Sparse-controlled gaussian splatting for editable dynamic scenes. *arXiv preprint arXiv:2312.14937*, 2023.
- [60] Zhan Li, Zhang Chen, Zhong Li, and Yi Xu. Spacetime gaussian feature splatting for real-time dynamic view synthesis. *arXiv preprint arXiv:2312.16812*, 2023.
- [61] Quankai Gao, Qiangeng Xu, Zhe Cao, Ben Mildenhall, Wenchao Ma, Le Chen, Danhang Tang, and Ulrich Neumann. Gaussianflow: Splatting gaussian dynamics for 4d content creation. *arXiv preprint arXiv:2403.12365*, 2024.
- [62] Youtian Lin, Zuoqiuo Dai, Siyu Zhu, and Yao Yao. Gaussian-flow: 4d reconstruction with dynamic 3d gaussian particle. *arXiv preprint arXiv:2312.03431*, 2023.
- [63] Shuaifeng Zhi, Tristan Laidlow, Stefan Leutenegger, and Andrew J Davison. In-place scene labelling and understanding with implicit scene representation. In *Proceedings of the IEEE/CVF International Conference on Computer Vision*, pages 15838–15847, 2021.
- [64] Xiao Fu, Shangzhan Zhang, Tianrun Chen, Yichong Lu, Lanyun Zhu, Xiaowei Zhou, Andreas Geiger, and Yiyi Liao. Panoptic nerf: 3d-to-2d label transfer for panoptic urban scene segmentation. In *2022 International Conference on 3D Vision (3DV)*, pages 1–11, 2022.
- [65] Abhijit Kundu, Kyle Genova, Xiaoqi Yin, Alireza Fathi, Caroline Pantofaru, Leonidas J. Guibas, Andrea Tagliasacchi, Frank Dellaert, and Thomas Funkhouser. Panoptic neural fields: A semantic object-aware neural scene representation. In *Proceedings of the IEEE/CVF Conference on Computer Vision and Pattern Recognition (CVPR)*, pages 12871–12881, June 2022.
- [66] Yawar Siddiqui, Lorenzo Porzi, Samuel Rota Bulò, Norman Müller, Matthias Nießner, Angela Dai, and Peter Kotschieder. Panoptic lifting for 3d scene understanding with neural fields. In *2023 IEEE/CVF Conference on Computer Vision and Pattern Recognition (CVPR)*, pages 9043–9052, 2023.
- [67] Bing Wang, Lu Chen, and Bo Yang. Dm-nerf: 3d scene geometry decomposition and manipulation from 2d images, 2023.
- [68] V. Tschernozki, I. Laina, D. Larlus, and A. Vedaldi. Neural feature fusion fields: 3d distillation of self-supervised 2d image representations. In *2022 International Conference on 3D Vision (3DV)*, pages 443–453, Los Alamitos, CA, USA, sep 2022. IEEE Computer Society.

- [69] Sosuke Kobayashi, Eiichi Matsumoto, and Vincent Sitzmann. Decomposing nerf for editing via feature field distillation. In S. Koyejo, S. Mohamed, A. Agarwal, D. Belgrave, K. Cho, and A. Oh, editors, *Advances in Neural Information Processing Systems*, volume 35, pages 23311–23330. Curran Associates, Inc., 2022.
- [70] Justin Kerr, Chung Min Kim, Ken Goldberg, Angjoo Kanazawa, and Matthew Tancik. Lurf: Language embedded radiance fields. In *Proceedings of the IEEE/CVF International Conference on Computer Vision (ICCV)*, pages 19729–19739, October 2023.
- [71] Rahul Goel, Dhawal Sirikonda, Saurabh Saini, and P. J. Narayanan. Interactive segmentation of radiance fields. In *Proceedings of the IEEE/CVF Conference on Computer Vision and Pattern Recognition (CVPR)*, pages 4201–4211, June 2023.
- [72] Alec Radford, Jong Wook Kim, Chris Hallacy, Aditya Ramesh, Gabriel Goh, Sandhini Agarwal, Girish Sastry, Amanda Askell, Pamela Mishkin, Jack Clark, et al. Learning transferable visual models from natural language supervision. In *International conference on machine learning*, pages 8748–8763. PMLR, 2021.
- [73] Boyi Li, Kilian Q Weinberger, Serge Belongie, Vladlen Koltun, and Rene Ranftl. Language-driven semantic segmentation. In *International Conference on Learning Representations*, 2022.
- [74] Mathilde Caron, Hugo Touvron, Ishan Misra, Hervé Jégou, Julien Mairal, Piotr Bojanowski, and Armand Joulin. Emerging properties in self-supervised vision transformers. In *Proceedings of the IEEE/CVF international conference on computer vision*, pages 9650–9660, 2021.
- [75] Minghan Qin, Wanhua Li, Jiawei Zhou, Haoqian Wang, and Hanspeter Pfister. Langsplat: 3d language gaussian splatting. 2024.
- [76] Chung Min Kim, Mingxuan Wu, Justin Kerr, Ken Goldberg, Matthew Tancik, and Angjoo Kanazawa. Garfield: Group anything with radiance fields, 2024.
- [77] Chen Yang, Sikuang Li, Jiemin Fang, Ruofan Liang, Lingxi Xie, Xiaopeng Zhang, Wei Shen, and Qi Tian. Gaussianobject: Just taking four images to get a high-quality 3d object with gaussian splatting. *arXiv preprint arXiv:2402.10259*, 2024.
- [78] Yi-Ling Qiao, Alexander Gao, and Ming Lin. Neuphysics: Editable neural geometry and physics from monocular videos. In S. Koyejo, S. Mohamed, A. Agarwal, D. Belgrave, K. Cho, and A. Oh, editors, *Advances in Neural Information Processing Systems*, volume 35, pages 12841–12854. Curran Associates, Inc., 2022.
- [79] Wang Yifan, Felice Serena, Shihao Wu, Cengiz Öztireli, and Olga Sorkine-Hornung. Differentiable surface splatting for point-based geometry processing. *ACM Transactions on Graphics (TOG)*, 38(6):1–14, 2019.
- [80] Ashish Vaswani, Noam Shazeer, Niki Parmar, Jakob Uszkoreit, Llion Jones, Aidan N Gomez, Łukasz Kaiser, and Illia Polosukhin. Attention is all you need. *Advances in neural information processing systems*, 30, 2017.
- [81] Tianye Li, Mira Slavcheva, Michael Zollhoefer, Simon Green, Christoph Lassner, Changil Kim, Tanner Schmidt, Steven Lovegrove, Michael Goesele, Richard Newcombe, et al. Neural 3d video synthesis from multi-view video. In *Proceedings of the IEEE/CVF Conference on Computer Vision and Pattern Recognition*, pages 5521–5531, 2022.
- [82] Adam Paszke, Sam Gross, Francisco Massa, Adam Lerer, James Bradbury, Gregory Chanan, Trevor Killeen, Zeming Lin, Natalia Gimelshein, Luca Antiga, Alban Desmaison, Andreas Kopf, Edward Yang, Zachary DeVito, Martin Raison, Alykhan Tejani, Sasank Chilamkurthy, Benoit Steiner, Lu Fang, Junjie Bai, and Soumith Chintala. Pytorch: An imperative style, high-performance deep learning library. In H. Wallach, H. Larochelle, A. Beygelzimer, F. d’Alché-Buc, E. Fox, and R. Garnett, editors, *Advances in Neural Information Processing Systems*, volume 32. Curran Associates, Inc., 2019.
- [83] Zhengqi Li, Simon Niklaus, Noah Snavely, and Oliver Wang. Neural scene flow fields for space-time view synthesis of dynamic scenes. In *Proceedings of the IEEE/CVF Conference on Computer Vision and Pattern Recognition*, pages 6498–6508, 2021.
- [84] Jonathan T Barron, Ben Mildenhall, Matthew Tancik, Peter Hedman, Ricardo Martin-Brualla, and Pratul P Srinivasan. Mip-nerf: A multiscale representation for anti-aliasing neural radiance fields. In *Proceedings of the IEEE/CVF International Conference on Computer Vision*, pages 5855–5864, 2021.

A Appendix / supplemental material

A.1 Introductions

The appendix provides some implementation details and further results that accompany the paper.

- Section A.2 introduces the implementation details of our temporal identity field network architecture.
- Section A.3 provides more descriptions including pseudocode of our approach.
- Section A.4 provides per-scene quantitative results.
- Section A.5 provides more visualization results.
- Section A.6 discusses the limitations of our approach.
- Section A.7 provides the implementation details and visualizations of mask annotation.
- Section A.8 provides more discussions.

A.2 Network Architecture of the Temporal Identity Field

The architecture of the temporal identity field network \mathcal{F}_θ are shown in Fig.8. The network is a simple MLP that takes time and the spatial positions of 3D Gaussians as inputs and outputs their corresponding identity encoding: $\mathcal{F}_\theta(\gamma(\mathcal{X}), \gamma(t)) = e$, where γ denotes the positional encoding. Specifically, the network concatenates $\gamma(\mathcal{X})$ and $\gamma(t)$, passes them through three fully connected ReLU layers, each with 256 channels, and outputs a 256-dimensional feature vector. Then, an additional fully connected layer is applied to map the feature vector to the final 32-dimensional identity encoding.

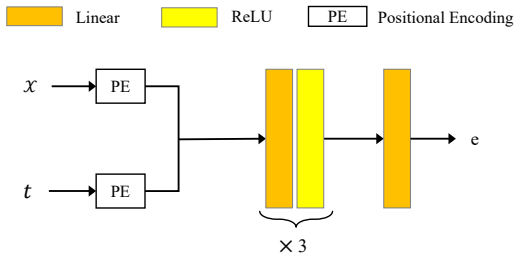


Figure 8: The architecture of our temporal identity field network.

A.3 More Algorithm Descriptions

We outline the pseudocode of training and 4D segmentation refinement for our SA4D in Algorithm 1 and Algorithm 2.

A.4 More Results

In Tab. 4 and Tab. 5, we provide the results for individual scenes associated with Sec. 5.2 of the main paper.

A.5 More Visualizations

We present more visualization results in Fig. 9, Fig. 10 and Fig. 11, showing the effectiveness of our method. Our method can not only render anything masks at novel views and novel timestamps but also segment single or multiple objects in 4D dynamic scenes.

Algorithm 1 SA4D Training Framework

$(\hat{M}_1, \hat{M}_2, \dots, \hat{M}_N) \leftarrow$ Zero-shot Video Segmentation \triangleright Pseudo Label
 $\mathcal{G}, \mathcal{F} \leftarrow$ InitPretrained4DGS() \triangleright Canonical 3D Gaussians and Deformation Field Network
 $\phi_\theta, \phi_c \leftarrow$ Init() \triangleright Temporal Identity Field Network and Convolutional Decoder
 $i \leftarrow 0$ \triangleright Iteration Count

while not converged **do**

$V, t, \hat{I}, \hat{M} \leftarrow$ SampleTrainingView() \triangleright Camera View, Timestamp, Image and Mask

$\mathcal{G}' \leftarrow \mathcal{F}(\mathcal{G}, t)$ \triangleright Deformed Gaussians

$e \leftarrow \phi_\theta(\gamma(\mathcal{X}), \gamma(t))$ \triangleright Compute Identity Encoding

$E \leftarrow$ Rasterize(\mathcal{G}' , e) \triangleright Rendered Identity Encoding

$L \leftarrow \lambda_{2d}L_{2d}(E, \hat{M}) + \lambda_{3d}L_{3d}(e)$ \triangleright Optimization Loss, see Eq. (13) and Eq. (14) of the paper

$\phi_\theta, \phi_c \leftarrow$ Adam(∇L) \triangleright Backprop & Step

$i \leftarrow i + 1$.

end while

return \mathcal{G}

Algorithm 2 4D Segmentation Refinement

Input: Temporal identity field network ϕ_θ , Classifier head ϕ_c , canonical 3D Gaussians \mathcal{G} , deformation field network \mathcal{F} , selected object IDs l , timestamp interval k , training images \hat{I} , corresponding camera views V , timestamps t and segmentation masks \hat{M}

Output: Gaussian identity table \mathcal{M} .

procedure REFINEMENT($\phi_\theta, \phi_c, \mathcal{G}, \mathcal{F}, l, k, \hat{I}, V, t, \hat{M}$)

$i \leftarrow 0$ \triangleright Iteration Count

while $i \leq N$ **do** \triangleright Enumerate training views

$V_i, t_i, \hat{I}_i, \hat{M}_i \leftarrow$ SampleTrainingView(i) \triangleright Camera View, Timestamp, Image and Mask

$\mathcal{G}' \leftarrow \mathcal{F}(\mathcal{G}, t_i)$ \triangleright Deformed Gaussians

$e \leftarrow \phi_\theta(\gamma(\mathcal{X}), \gamma(t_i))$ \triangleright Compute Identity Encoding

$\hat{\mathcal{G}} \leftarrow \phi_c(e)$ \triangleright Classified 3D Gaussians

$\mathcal{G}_l \leftarrow$ SelectGaussians($\hat{\mathcal{G}}, l$) \triangleright Segment target Gaussians

$\mathcal{G}_l \leftarrow$ RemoveOutliers($\mathcal{X}, \mathcal{G}_l$) \triangleright Remove Outliers

$m \leftarrow \mathbb{I}(g \in \mathcal{G}_l)$ \triangleright Initialize 3D Point Masks

$M \leftarrow$ Rasterize(\mathcal{G}' , m) \triangleright Rendered Object Mask

$L \leftarrow L_{proj}(M, \hat{M}_i)$ \triangleright Mask Projection Loss, see Eq. (15) of the paper

$G_m \leftarrow \nabla L$ \triangleright Gradients of 3D Point Masks

for g_m in G_m **do** \triangleright Remove Ambiguous Gaussians at the Boundary

if $g_m < 0$ **then**

$\mathcal{G}_l \leftarrow$ RemoveGaussian()

end if

end for

$\mathcal{M} \leftarrow$ Store(\mathcal{G}_l, t_i) \triangleright Update the Gaussian Identity Table

$i \leftarrow i + k$

end while

return \mathcal{M}

end procedure

Method	split-cookie		chickchicken		torchocolate	
	IoU(%)	Acc(%)	IoU(%)	Acc(%)	IoU(%)	Acc(%)
SAGA [4]	51.99	56.78	68.88	72.75	58.45	60.36
Gaussian Grouping [6]	57.87	90.68	80.43	98.41	68.02	89.15
Ours w/o TFF (w/o Refinement)	76.89	99.82	90.73	99.03	74.00	99.19
Ours w/ TFF (w/o Refinement)	83.31	99.82	88.85	99.00	74.95	99.03
Ours w/ all	88.92	99.73	92.57	98.53	88.92	98.34

Method	espresso		keyboard		americano	
	IoU(%)	Acc(%)	IoU(%)	Acc(%)	IoU(%)	Acc(%)
SAGA [4]	57.64	98.22	73.65	78.01	80.91	87.22
Gaussian Grouping [6]	62.36	79.66	74.77	93.32	73.71	98.08
Ours w/o TFF (w/o Refinement)	72.39	99.88	86.72	99.44	80.80	99.99
Ours w/ TFF (w/o Refinement)	74.11	99.89	82.87	99.52	82.48	99.98
Ours w/ all	88.42	99.73	90.73	99.19	89.60	99.91

Table 4: Quantitative results on the HyperNeRF [18] dataset. ‘‘Ours w/o TF’’ means directly attaching an identity feature vector to each Gaussian.

Method	cut roasted beef		flame steak		cook spinach	
	IoU(%)	Acc(%)	IoU(%)	Acc(%)	IoU(%)	Acc(%)
SAGA [4]	74.25	76.11	78.33	81.26	78.66	81.57
Gaussian Grouping [6]	84.86	93.74	88.94	99.87	85.60	99.06
Ours w/o. Refinement	85.05	99.97	76.14	99.82	82.01	99.97
Ours	94.09	99.88	92.63	99.40	92.33	99.75

Method	flame salmon		coffee martini		sear steak	
	IoU(%)	Acc(%)	IoU(%)	Acc(%)	IoU(%)	Acc(%)
SAGA [4]	75.39	78.21	77.97	82.40	72.96	89.79
Gaussian Grouping [6]	87.41	99.93	89.53	99.82	85.78	99.89
Ours w/o Refinement	78.43	99.85	83.28	99.67	75.95	99.98
Ours w/ all	93.10	99.77	93.07	99.80	92.91	99.93

Table 5: Quantitative results on the Neu3D [81] dataset.

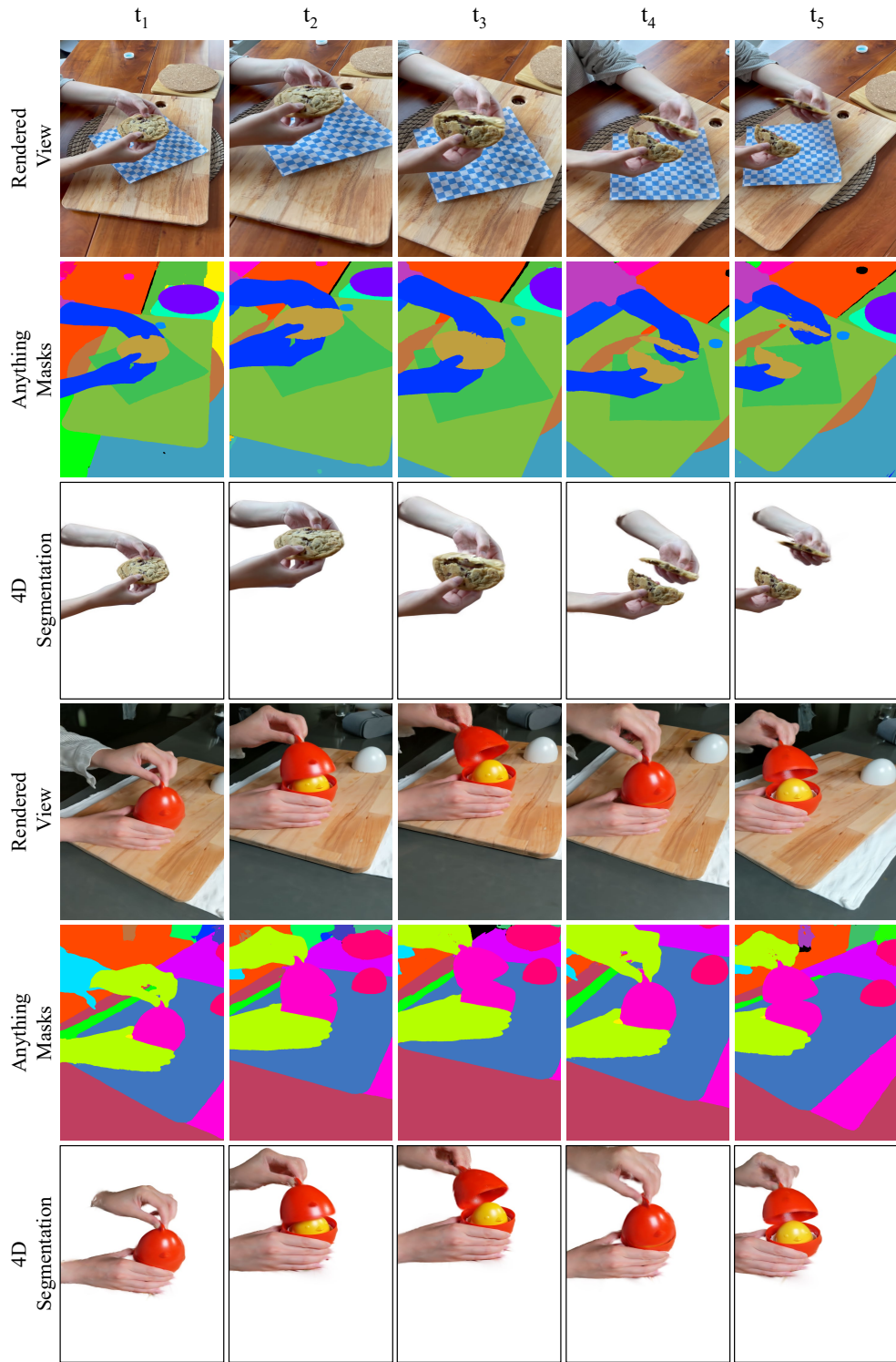


Figure 9: More visualizations results.

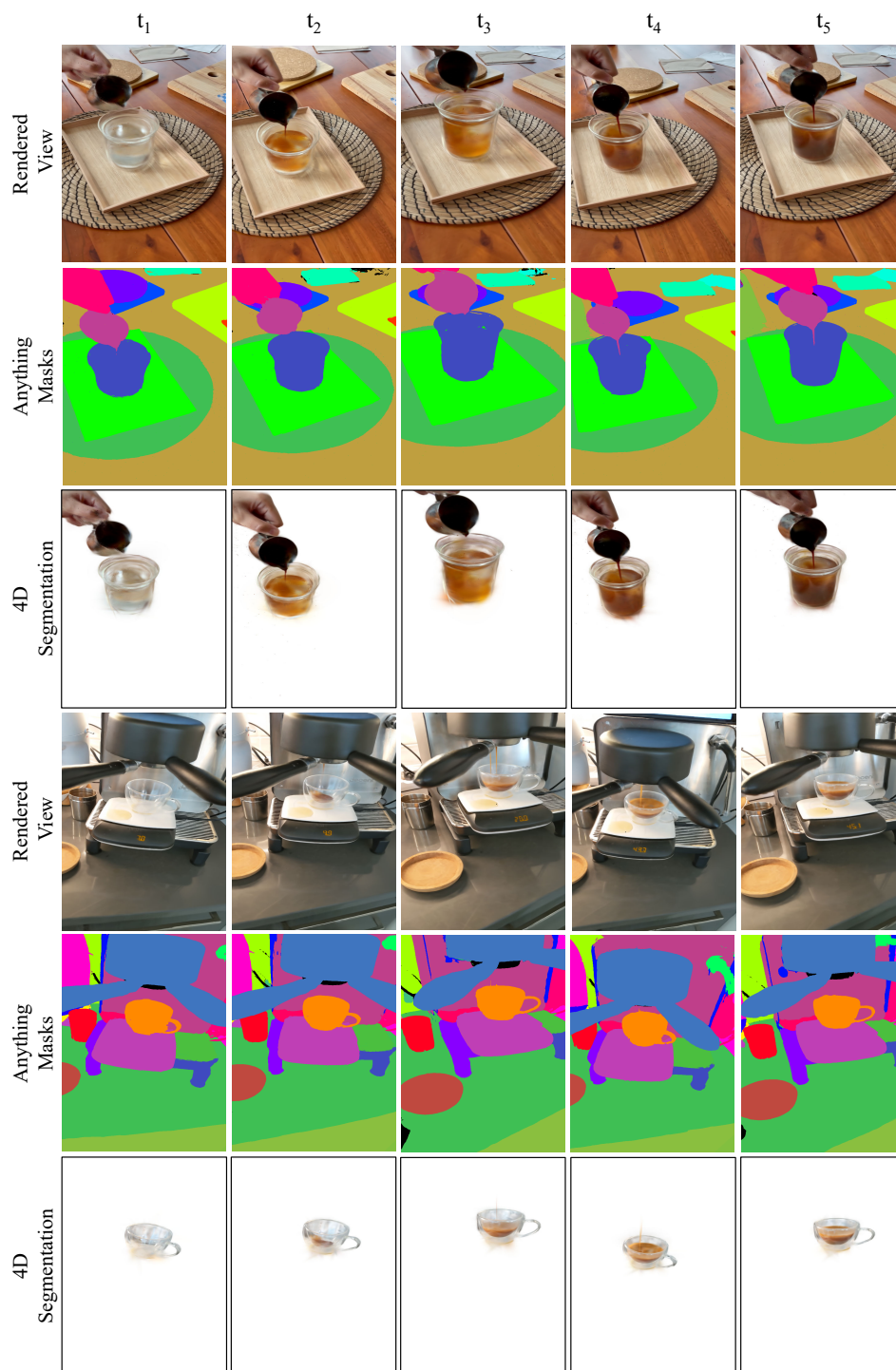


Figure 10: More visualizations results.

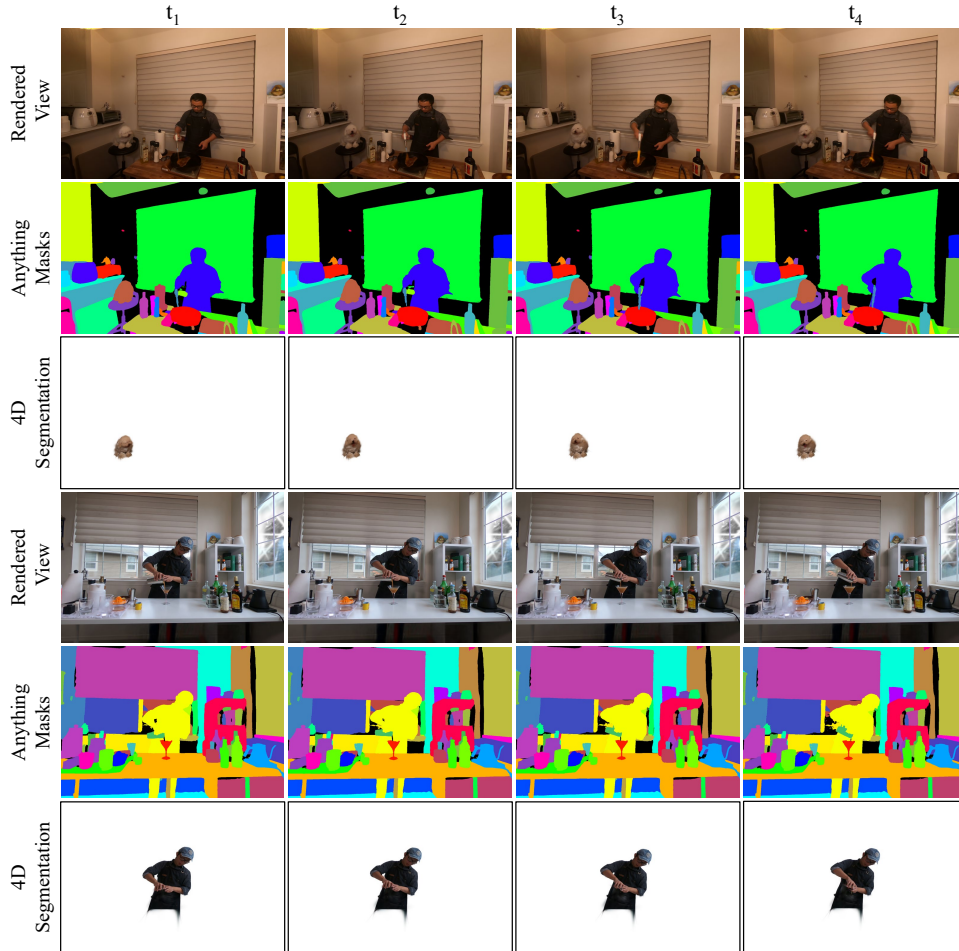


Figure 11: More visualizations results.

A.6 More Limitations

4D Segmentation Refinement. In the 4D segmentation refinement, we utilize the segmentation mask of zero-shot video segmentation model [17] as prior to remove ambiguous Gaussians at the boundary. However, [17] sometimes fail to generate correct segmentation masks, which leads to the failure of the 4D segmentation refinement. As illustrated in Fig. 12, since zero-shot video segmentation model labels the cup as void (the black region in the yellow box) at timestamp 0 by mistake, the whole cup is removed after refinement.

Mask Identity Collision in Multi-view Settings. In the Neu3D Dataset, we only use the image sequence under one camera view rather than multiple views for training due to the Mask Identity Collision, in which video tracker [17] assigns different ID to the same object in different video inputs. However, training with a single view may result in inferior anything masks when rendered in novel views, as shown in Fig. 13. Moreover, 3D segmentation results without any refinement at each timestamp may also contain lots of noise due to heavy occlusion in a single view.

A.7 Mask Annotation

As there are no ground truth segmentation mask labels for HyperNerf [18] and Neu3D [81] datasets, we manually annotate 6 scenes from HyperNerf and all scenes from Neu3D. We use the Roboflow platform and SAM [1] for interactive mask annotation. For each scene, we choose 20-30 frames in

the test dataset and annotate object masks for measuring the segmentation accuracy. We provide some visualization examples of mask annotations in Fig. 14.

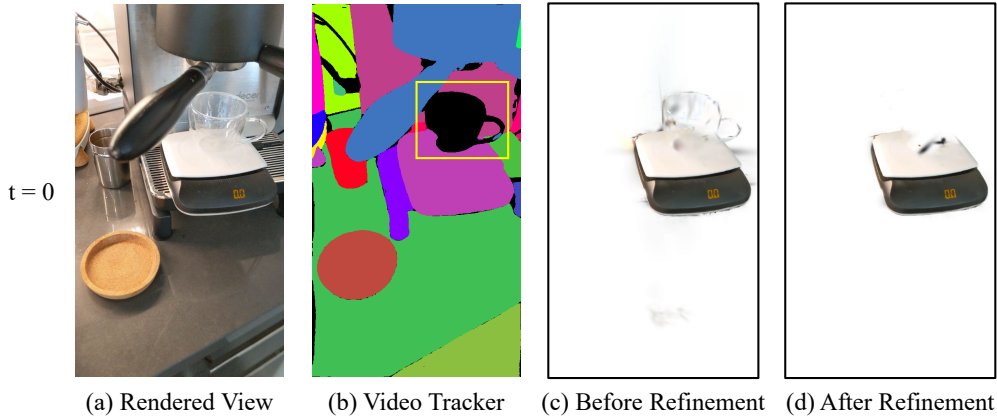


Figure 12: The failure case of 4D segmentation refinement.

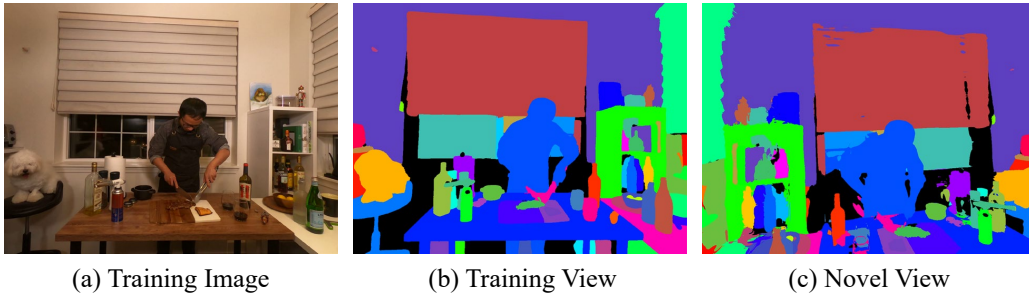


Figure 13: Novel view anything mask rendering results in the Neu3D [81] dataset.

A.8 More discussions

Training 4D-GS with semantic features. There are several approaches [63, 6] demonstrate that optimizing the scene with a semantic feature simultaneously may trigger the downgrade of rendering novel views. It is mainly because the object semantic feature may enforce the Gaussian included in o have similar features. Therefore, our SA4D adopts two-stage training: training deformation field \mathcal{F} and canonical 3D-GS \mathcal{G} at first, then optimizing temporal identity feature field network by freezing the weight of \mathcal{F} and \mathcal{G} .

May SA4D help monocular dynamic scene reconstruction? Similar to GaussianObject [77], SA3D/SAGA is used to generate the object’s mask, and the repair process is proposed to repair the 3D object. We believe that SA4D can also support the reconstruction in the monocular setups and leave it as future work.

Social impacts. SA4D shows the ability of composition with 4D Gaussians. The rendered image achieves photo-realistic performance. To mitigate the societal impact of highly realistic technology, several measures can be taken. Technologically, embedding watermarks or digital signatures and developing detection algorithms can ensure image authenticity. Legally, implementing regulations and strict enforcement can deter malicious activities. Educating the public on media literacy enhances their ability to discern real from fake images. Social media platforms must enforce rigorous content review and provide easy reporting mechanisms. Lastly, industry self-regulation and ethical training for practitioners can promote responsible 4D composition/editing practices.

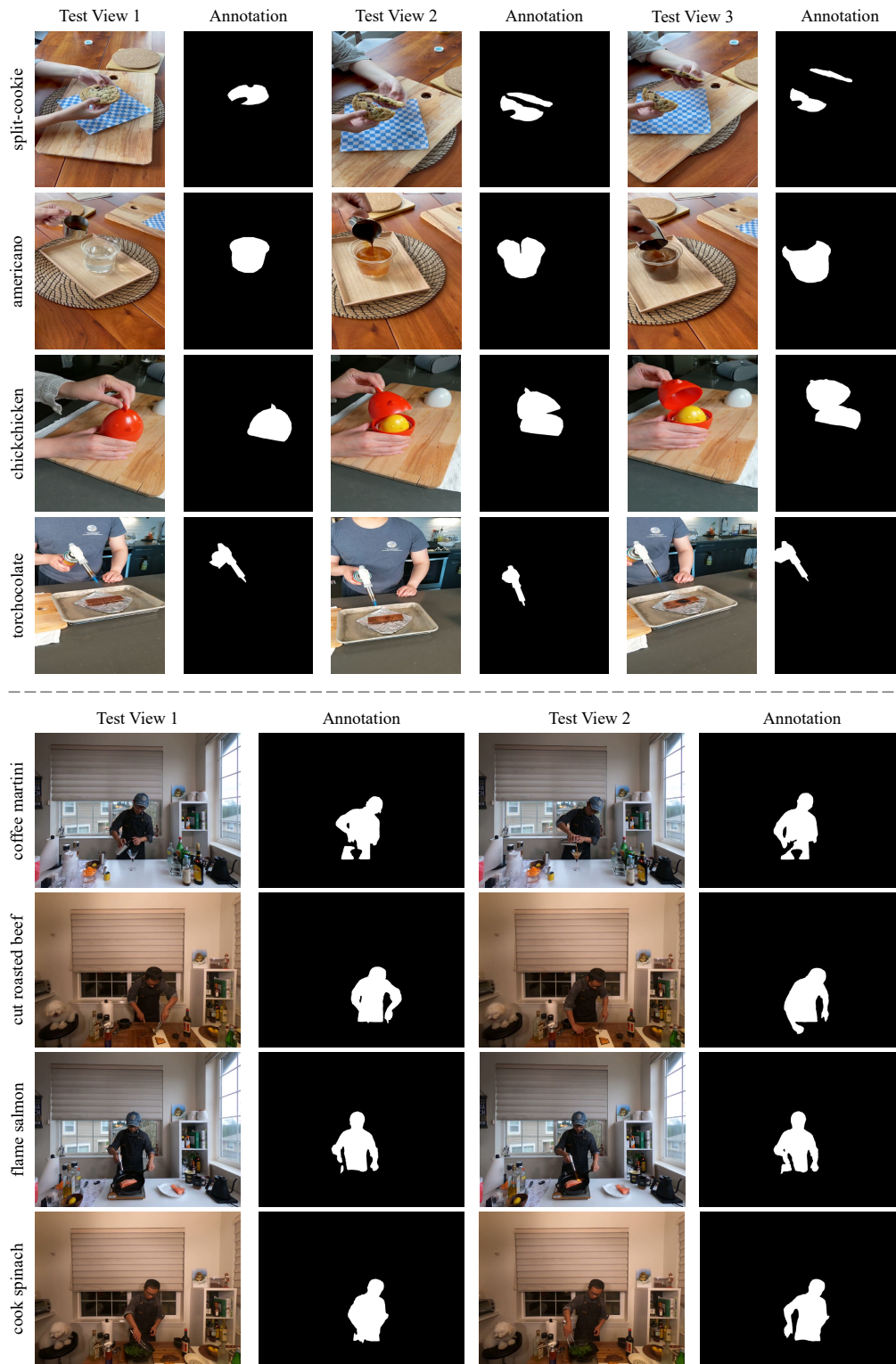


Figure 14: Visualizations of mask annotations. The top four rows are from the HyperNeRF [18] dataset and the bottom four rows are from the Neu3D [81] dataset.